3. Levels in Hf^{179} and Hf^{181}

Only two gamma lines have been observed in each of these isotopes. Their energies and intensities are shown in Table III. When the Hf^{179} lines are compared with the Hf^{181} lines, both isotopes are seen to show intense $E1$ transitions from the capture state (a $\frac{1}{2}^+$ state in each case) to a low-lying $\frac{1}{2}^-$ state (the $\frac{1}{2}^-$ isomeric level at 378 keV in Hf^{179} and the $\frac{1}{2}^-$ ground state in Hf^{181}), and also a somewhat less intense (but still strong) transition from the capture state to a level just above the $\frac{1}{2}^-$ level. The spacing from the $\frac{1}{2}^-$ level to the level just above it is about the same in both isotopes —44 keV in Hf^{179} and 47 keV in Hf^{181}. The levels which we observed in Hf^{179} have also been observed in (d,p) work and have been identified with the $\frac{1}{2}^-$ and $\frac{3}{2}^-$ levels in the $\frac{1}{2}^-(510)$ Nilsson band.[7] The present data suggest that the ground state and 47-keV state, to which we have observed transitions in Hf^{181}, are the $\frac{1}{2}^-$ and $\frac{3}{2}^-$ levels in the $\frac{1}{2}^-(510)$ band.

It is interesting to see how our measurements on Hf^{179} and Hf^{181} compare with known data on W^{183}. The latter has the same number of neutrons as Hf^{181}, differing only in that it has an additional pair of protons. The ground state of W^{183}, like that of Hf^{181}, is a $\frac{1}{2}^-(510)$ state; and this isotope has intense $E1$ transitions from the capture state to the $\frac{1}{2}^-$ and $\frac{3}{2}^-$ levels in the $\frac{1}{2}^-(510)$ band. The transition rates are 13% and 3%, respectively.[11] The ratio (4.3:1) of these two intensities in W^{183} agrees fairly well with the ratios (5.9:1 and 3.4:1) for the corresponding transitions in Hf^{179} and Hf^{181}, respectively. The energy separation between the $\frac{1}{2}^-$ and $\frac{3}{2}^-$ levels in the (510) band of W^{183} is 46 keV, which is close to the (44±3)-keV separation in Hf^{179} and the (47±3)keV separation in Hf^{181}.

ACKNOWLEDGMENTS

We would like to acknowledge our indebtedness to H. Mann and his co-workers who provided us with the germanium detectors and gave us much assistance during this work.

[11] G. A. Bartholomew, J. W. Knowles, and P. J. Campion, Atomic Energy Commission, Ltd. Report No. AECL-954-43, 1960 (unpublished).

PHYSICAL REVIEW VOLUME 146, NUMBER 3 17 JUNE 1966

Further Study of Nuclear Resonant Scattering Using Neutron-Capture Gamma Rays

G. Ben-David, B. Arad, J. Balderman, and Y. Schlesinger
Nuclear Physics Department, Israel Atomic Energy Commission, Soreq Nuclear Research Center, Yavne, Israel

(Received 11 October 1965)

The study of resonance scattering of neutron-capture gamma rays has been extended using 22 capture gamma sources and 57 scattering targets. About 50 resonance-scattering events have been observed in 23 elements and the effective cross sections evaluated. Some cases of complex spectra are described. The association of the scattering with nuclei in the region of closed shells is clearly shown. Problems of minimum observable cross sections are discussed and some further applications of the technique are suggested.

INTRODUCTION

MANY instances of nuclear resonant scattering of gamma rays have been observed[1–4] when various elements are irradiated with monoenergetic neutron-capture gamma rays. Resonant scattering occurs when the energy of the gamma ray (after correction for target recoil) happens to overlap, partially or entirely, an individual nuclear level in the target nucleus. In the works referred to above the scattered spectra, in the energy range 6–9 MeV, were measured using sodium-iodide detectors positioned at an angle of 135° to the incident radiation. Despite the poor energy resolution of these detectors—which permitted the determination of the peak energy with a precision of only 50 keV—it was usually possible to identify unambiguously the particular capture gamma-ray line responsible for the resonance, using the published tabulations[5] of capture gamma rays, and thence to determine the energy of the resonant level in the target nucleus to the same accuracy as that of the known gamma line, i.e., to within 10 keV in most cases. A comparison of the intensity of the scattered and incident beam, permitted an evaluation of the effective

[1] G. Ben-David and B. Huebschmann, Phys. Letters 3, 82, (1962).
[2] B. Arad, G. Ben-David, I. Pelah, and Y. Schlesinger, Phys. Rev. 133, B684 (1964).
[3] H. H. Fleischmann, Ann. Physik 12, 133 (1963).
[4] C. S. Young and D. I. Donahue, Phys. Rev. 133, 1724 (1963).

[5] *Nuclear Data Sheets*, complied by K. Way *et al.* (Printing and Publishing Office, National Academy of Sciences–National Research Council, Washington 25, D. C.).

scattering cross section. This technique has permitted the identification of highly excited nuclear levels, and in favorable cases an estimation of the level widths.

In the present work the study of resonant scattering has been extended using additional capture-gamma-ray sources and targets. Some 50 resonance events have now been found and evaluated.

EXPERIMENTAL METHOD

The experimental arrangement used is as described in Ref. 2 except for a few minor changes in the electronic equipment designed to give improved stability and energy resolution. The Dumont 6363 photomultiplier was replaced by a venetian-blind-type tube RCA 8054, used with a "Spectrastat" spectrum stabilizer power supply "locked" on the 2.6-MeV ThC gamma line. These changes gave an improved energy resolution with a precision in determination of the peak energy improved to 25 keV, permitting more precise analysis of the spectra and, in cases of doubt, more certain identification of the resonant capture gamma line.

The additional scatterers were prepared as in the earlier work. However, the preparation of the thallium targets raised some technical difficulties because of the highly toxic nature of thallium. As a precaution against health hazards the thallium was cast into thin stainless-steel containers, located in a closed vessel. The process was carried out under an argon atmosphere to eliminate the hazard from the formation of the oxide during casting.

The gamma beam was obtained by placing a suitable source at an appropriate position in the reactor thermal column, the beam reaching the target through an access hole in the shielding wall. It was found that during the early experiments a relatively large number of neutrons reached the steel framework of the access hole due to a faulty fitting of the borated plastic plugs designed to prevent leakage of neutrons from the thermal column. This resulted in a background of iron-capture gamma rays which, while not noticeable in the direct spectra of the various capture gamma sources, caused the appearance of weak spurious resonances in the experiments with lead targets, owing to the very strong resonance of the iron 7.285-MeV line in lead (effective cross section 4 b). This fault has now been corrected and the previously published resonances carefully remeasured. The effective cross sections for resonant scattering have been evaluated for these resonances, as well as for the new ones reported in this work, using Eqs. (8a) and (8b) of Ref. 2. These formulas apply strictly to targets consisting of one element only, the effective cross section being averaged over all the isotopes present. For targets consisting of chemical compounds the appropriate formulas for the effective cross sections are as follows:

$\sigma_n \ll \sigma_e$:

$$\langle\sigma_{\gamma\gamma}\rangle=\frac{C_{sc}}{C_0}\frac{\eta_0}{\eta_{sc}}\frac{11.2}{\Delta\Omega}\frac{1+\sqrt{2}}{s^0}\times\frac{\sum_i s^i\sigma_e{}^i}{1-\exp[-(1+\sqrt{2})Nx_0\sum s^i\sigma_e{}^i]}; \quad (1a)$$

$\sigma_n \gtrsim \sigma_e$ [only applicable for a thin scatterer, where $Nx_0(\sigma_n+\sigma_e)\ll 1$]:

$$\langle\sigma_{\gamma\gamma}\rangle=\frac{C_{sc}}{C_0}\frac{\eta_0}{\eta_{sc}}\frac{11.2}{\Delta\Omega}\frac{1}{s^0Nx_0}\frac{2}{2-(1+\sqrt{2})Nx_0\sum s^i\sigma_e{}^i}, \quad (1b)$$

where σ_n is the total nuclear cross section, σ_e is the total electronic cross section, $\langle\sigma_{\gamma\gamma}\rangle$ is the effective resonant-scattering cross section, C_{sc} is the counting rate of the scattered beam under the photopeak, C_0 is the corresponding counting rate in the direct spectrum, η_0 and η_{sc} are the photofraction for direct and scattered radiation, respectively; 11.2 is the factor taking into account the scattering angle of 135° (for an assumed dipole distribution of scattered radiation), $\Delta\Omega$ is the average solid angle subtended by the detector, s^i is the number of atoms of element i per target molecule, s^0 is the corresponding number of atoms of the resonant element, N is the number of target molecules per unit volume, and x_0 is the target thickness in cm.

EXPERIMENTAL RESULTS AND ANALYSIS

Full details of the sources and targets used in the general survey of nuclear resonance scattering are summarized in Tables I and II. Of the 50 resonances observed the great majority appear to possess simple spectra, corresponding to a single gamma line. How-

TABLE I. Capture gamma-ray sources.

Source material	Chemical composition	Mass (kg)
Ag	metal	0.400
Al	metal	1.640
As	As_2O_5	0.250
Cl	polyvinyl chloride	0.380
Co	CoO	0.230
Cr	metallic powder	0.480
Cu	metal	1.860
Fe	metallic powder	0.440
Gd	Gd_2O_3	0.100
Hg	$Hg_2(NO_3)_2\cdot 2H_2O$	0.310
K	$K_2C_2O_4\cdot H_2O$	1.000
Mn	MnO	0.240
Ni	metal	0.900
Pb	metallic powder	1.000
S	powder	1.000
Se	metal	0.400
Sm	Sm_2O_3	0.200
Sr	$Sr(OH)_2\cdot 8H_2O$	0.250
Ti	TiO	0.210
V	V_2O_5	0.120
Y	Y_2O_3	0.200
Zn	metal	0.500

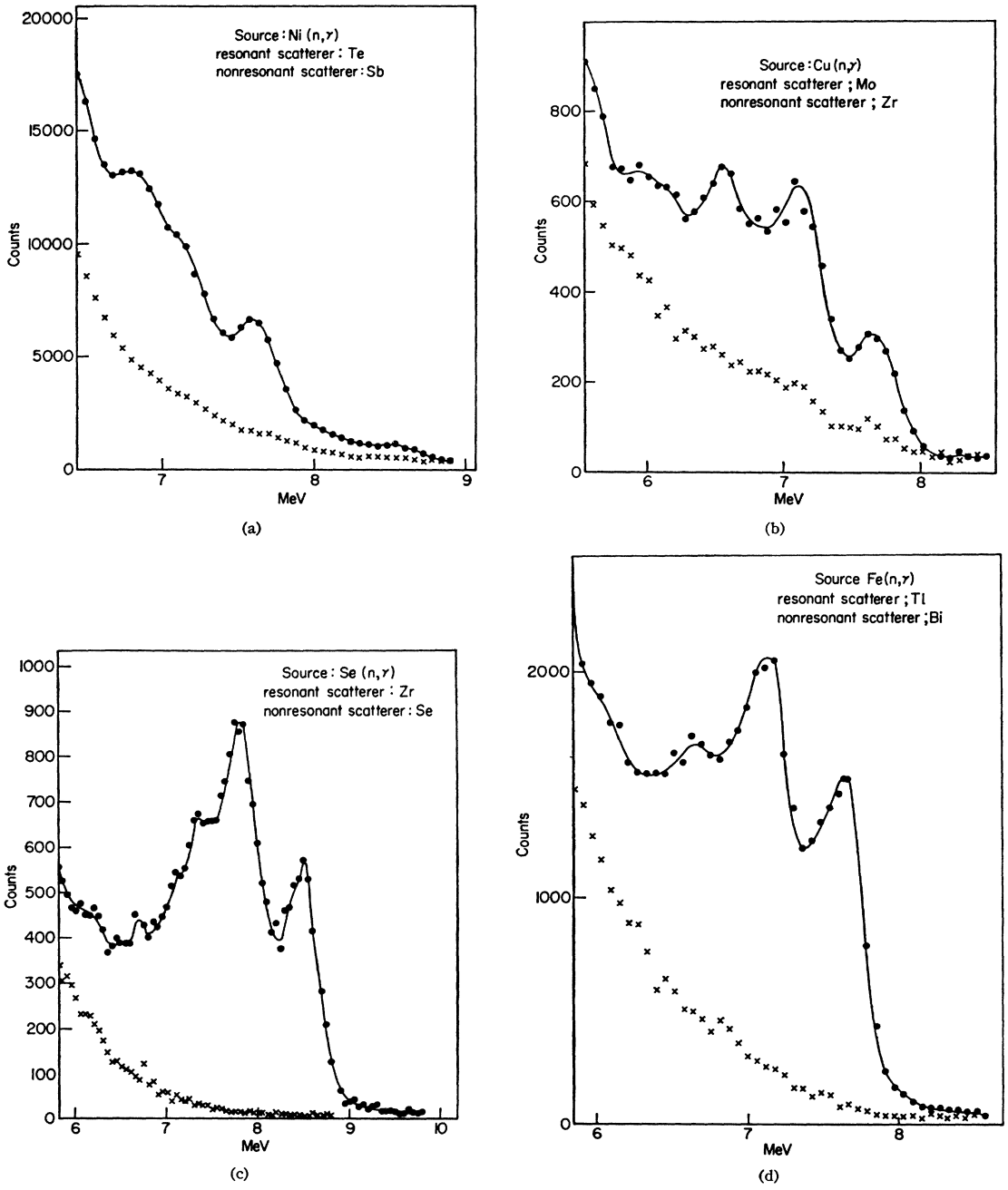

FIG. 1. (a) Complex scattered spectrum from Te excited by Ni capture gamma rays (with Sb background). (b) Complex scattered spectrum from Mo excited by Cu capture gamma rays (with Zr background). (c) Complex scattered spectrum from Zr excited by Se capture gamma rays (with Se background). (d) Simple scattered spectrum from Tl excited by Fe capture gamma rays (with Bi background).

ever some examples of complex scattered spectra were observed, where two or more gamma lines appear in the scattered beam. Typical examples are shown in Fig. 1, together with a simple spectrum for comparison. These complex spectra are caused either by scattering of two or more source lines by independent nuclear levels, by inelastic scattering events, or by a mixture of the two. Figure 2 shows the complex spectrum excited by Ni capture gamma rays on Te, which can be resolved into components at 8.5, 7.528, 6.7, and 5.0 MeV. These complex spectra are being studied using the coincidence technique, and in favorable cases of inelastic scattering it is hoped that the isotope responsible for the resonance can be identified by identification of the low-lying nuclear levels.

Several levels, including the 7.64-MeV level of

TABLE II. Scattering targets.

Scattering target	Chemical composition	Total thickness (g/cm^2)	Thickness parameter χ (barn)
Ag	metal	10.84	12
Al	metal	12.00	2
Au	metal	17.60	19
Ba	BaO	11.34	15
Bi	metal	14.44	20
Bi	metal	2.91	...
Br	NH_4Br	5.96	14
Ca	$CaCO_3$	2.03	36
Cd	metal	12.79	11
Ce	Ce_2O_3	12.12	15
Cl	polyvinyl chloride (CH_2CHCl)	6.50	9
Co	CoO	2.80	20
Cr	metallic powder	5.84	7
Cu	metal	13.20	5
Dy	Dy_2O_3	2.36	50
Er	Er_2O_3	2.37	50
Fe	metal	9.28	6
Gd	Gd_2O_3	2.38	50
Hf	metallic powder	2.41	60
Hg	$Hg(NO_3)_2 \cdot 2H_2O$	11.50	...
Hg	liquid metal	19.60	17
Ho	Ho_2O_3	2.37	50
I	crystalline	9.74	13.5
K	$K_2C_2O_4 \cdot H_2O$	4.45	16
La	La_2O_3	6.20	24
Mg	MgO_2	3.66	12
Mn	MnO_2	6.21	13
Mo	metallic powder	8.41	11
Na	$Na_2CO_3 \cdot H_2O$	4.34	10
Nd	Nd_2O_3	2.36	51
Ni	metal	10.99	6
P	powder	3.67	6
Pb	metal	15.84	19
Pb	metal	3.25	...
Pb^{206}	$PbCO_3$	8.48	...
Pr	Pr_2O_3	5.41	27
Pt	metal	17.00	17
S	powder	2.31	11
Sb	metallic powder	15.57	10
Se	metallic powder	3.57	18
Si	glass	11.37	5
Sm	Sm_2O_3	5.42	29
Sn	metal	10.84	12
Sr	$Sr(OH)_2 \cdot 8H_2O$	3.02	65
Ta	metallic powder	2.47	60
Te	metallic powder	15.30	11
Th	ThO_2	2.73	73
Ti	crushed sponge	3.48	11
Tl	metal	14.85	20
Tl	metal	3.81	...
U	UO_2Cl_2	3.63	78
V	V_2O_5	3.60	18
W	metal	8.10	26
Y	Y_2O_3	3.44	35
Yb	Yb_2O_3	2.34	65
Zn	metal	9.82	7
Zr	ZrO_2	8.10	14

thallium excited by iron-capture gamma rays, have been further studied using temperature variation and self-absorption techniques, to give information on the level widths. The experimental results are being evaluated and will be reported elsewhere.

It was possible to analyze 46 of the resonances, and obtain the effective cross sections, these being summarized in Table III. The cross sections were usually averaged over all the isotopes of the resonant element, with an accuracy of $\pm 20\%$. For calculating the relative line intensities the latest tabulated data of Bartholomew[5] were used.

The abundance of observed resonance events among the different scattering targets is shown in histogram form in Fig. 3. For the majority of multi-isotopic target nuclei it was not possible to determine the isotope responsible for a resonance event. However, in certain cases it was possible to reject those isotopes where the (γ,n) threshold was below the resonant energy. For example, in the case of the 8.997-MeV level in Sm,

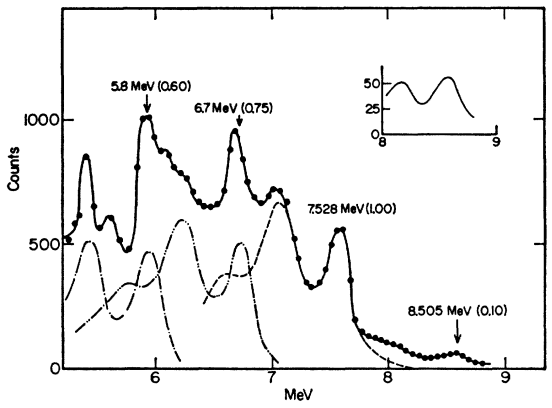

FIG. 2. The complex spectrum from Te resolved into separate components (figures in brackets give relative line intensities).

only the 82 neutron isotope has the (γ,n) threshold above this energy and it is thus possible to reject the 86, 87, 88, 90, and 92 neutron isotopes. A study of Fig. 3 shows that the distribution of resonances is not random, there being pronounced grouping at elements in the vicinity of closed shells of nucleons (shown in brackets). These effects appear predominantly in the region of the 50 proton and 82 proton shells, and the 50, 82, and 126 neutron shells. The large number of resonances found for La and Pr, both essentially mono-isotopic elements with 82 neutrons, strongly suggests that the 82 neutron isotopes are the ones responsible for the reso-

TABLE III. List of effective cross sections.

Scatterer	Energy (MeV)	Gamma source	δ (mb)	Scatterer	Energy (MeV)	Gamma source	δ (mb)
Sm^{144}	8.997	Ni	100	Sn	7.01	Cu	110
Pr^{141}	8.881	Cr	9	Nd	6.867	Co	30
La	8.532	Ni	6	Pr^{141}	6.867	Co	3
Te	8.532	Ni	3[a]	Te	6.7	Ni	...
Cu	8.499	Cr	24	La	6.54	Ag	12
Zr	8.496	Se	3050	Cd	6.474	Co	110
Zn	8.119	Ni	13	Mo	6.44	Hg	25[g]
Se	7.817	Ni	50	La	6.413	Ti	72
Se	7.76	K	90	Mo	6.413	Ti	10
Sb	7.67	V	...[b]	Tl	6.413	Ti	25
Cd	7.64	Fe	40[c]	W	~6.3	Ti	...[b]
Ni	7.64	Fe	7[c]	Sb	6.31	Hg	6[c]
Pr^{141}	7.64	Fe	12[c]	Ti	6.31	Hg	2[c]
Tl	7.64	Fe	370[c]	Sn	6.27	Ag	75
La	7.634	Cu	7	Pb^{206}	6.15	Gd	...[g]
Mo	7.634	Cu	11	Te	5.8	Ni	...[f]
Bi^{209}	7.634	Cu	4	La	6.12	Cl	35
Te	7.528	Ni	66[d]	Pr^{141}	6.12	Cl	110
Bi^{209}	7.416	Se	100	Pt	5.99	Hg	40[e,g]
Bi^{209}	7.300	As	80[e]	Tl	5.99	Hg	5[g]
Pb^{208}	7.285	Fe	4100	Pb^{206}	5.9	Sr	...[h]
Cl	7.285	Fe	34	Ce	5.646	Co	17
Pr^{141}	7.185	Se	80	Bi^{209}	5.646	Co	55
Tl	7.16	Cu	120	Pb^{208}	5.53	Ag	70
La	7.15	Mn	50	Hg	5.44	Hg	75[g]
Bi^{209}	7.149	Ti	2000	Hg	4.903	Co	385

[a] High-energy component of a complex spectrum.
[b] A broad scattered spectrum with no observable peak structure.
[c] There are actually two lines of energies 7.647 and 7.633 MeV having equal intensities in the iron capture gamma spectrum. The cross section has therefore been corrected, although there is no possibility at present of deciding which line is responsible for each resonance.
[d] Is probably an independent level in the complex spectrum of Ni γ rays on Te.
[e] Rough estimate.
[f] May be inelastic component from 7.528 level in Te.
[g] The relative line intensities in this case are due to Groshev and co-workers.
[h] No line is known for the source at this energy.
[i] Difficult to resolve among the many source lines present at this energy.

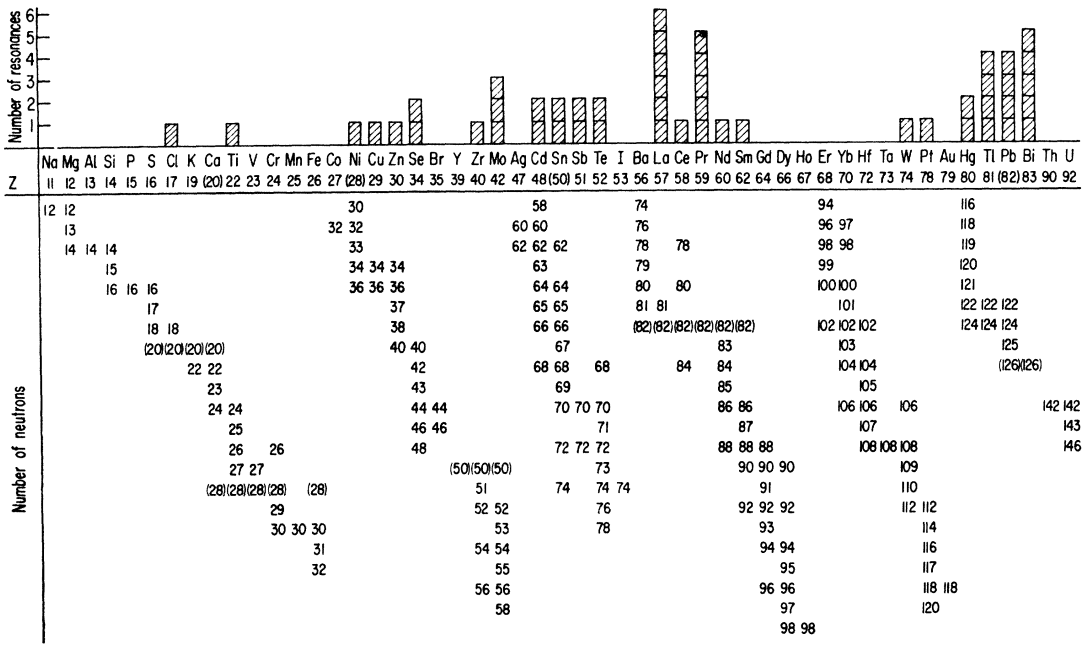

FIG. 3. Histogram of distribution of observed resonances among the different targets. The atomic number is given directly beneath the chemical symbol followed by the neutron numbers of the naturally occurring isotopes. Magic numbers are shown in brackets.

nances observed among the rare earths. It is significant that no resonances are observed among the seven medium-weight elements between Gd and Ta, although these possess a large number of isotopes having the (γ,n) threshold above the average gamma energies used. These seven elements have in common a large separation from regions of closed shells of nucleons. In fact, only in two cases (W,Pt) were resonances observed in elements not possessing isotopes within two nucleons of a closed shell.

Any interpretation of the above phenomenon must take into account the special nature of the gamma sources, which in effect comprise a large number of individual lines of widely differing intensities. These lines are quite sharp, the width being determined predominantly by the Doppler broadening caused by thermal motion of the source nuclei.[6] The line shape is given by the form $\exp\{-[E_\gamma-E)^2/\Delta_e^2)\}$, which expresses the intensity at energy E, for a peak gamma energy E_γ. The Doppler width Δ_e is equal to $E_\gamma(2kT_i/M_0c^2)^{1/2}$, where k is the Boltzmann constant, T_i is the effective temperature of the source,[7] and M_0c^2 is the rest mass of the source nucleus in energy units. For the different sources used in this experiment Δ_e varied between 4 and 8 eV. The effective cross section $\langle\sigma_{\gamma\gamma}\rangle$ for scattering one of these gamma lines from a particular nuclear level, is obtained by integrating the elastic scattering cross section over the incident gamma line spectrum; it has been shown[2] to be given by

$$\langle\sigma_{\gamma\gamma}\rangle=2\pi\lambda\!\!\!^{-2}g(\Gamma_0/\Gamma)^2\Psi(x_2,t_2)\,, \qquad (2)$$

where $\lambda\!\!\!^{-}$ is the gamma wavelength divided by 2π, g is the ratio of spin weight factors for the excited and ground states, Γ is the full width of the excited state, Γ_0 is the partial width for de-excitation to the ground state, and $\Psi(x,t)$ is the well-known "Doppler" integral[8] which corrects the Breit-Wigner cross section for thermal Doppler broadening. The parameters x_2 and t_2 are given by $x_2=2\delta/\Gamma$ and $t_2=(\Delta_e^2+\Delta^2)/\Gamma^2$, where δ is the energy separation between the gamma line and the resonant level peak (after correcting for target recoil), and Δ is the target Doppler width.

For a given energy region the parameters $\lambda\!\!\!^{-}$, Δ_e, and Δ are fixed for a given target and source. The variation of the effective cross section then depends only on the level parameters g, $(\Gamma_0/\Gamma)^2$, and on the energy separation δ. The variation in $\langle\sigma_{\gamma\gamma}\rangle$ as a function of δ is shown in Fig. 4 for three different values of Γ, namely 5, 1, and 0.2 eV. In this example the factor $g(\Gamma_0/\Gamma)^2$ was taken as unity, and $(\Delta_e^2+\Delta^2)$ as 80 $(\text{eV})^2$ a typical value for the sources and targets used. It can be seen from Fig. 4 that the maximum cross sections (at zero separation energy) are quite sensitive to the value of Γ, being equal to 18.6, 4.7, and 0.98 b, respectively, for the above three cases.

Since the energy separation δ between the resonant level and a gamma line is quite arbitrary, the prob-

[6] B. Arad, G. Ben-David, and Y. Schlesinger, Nucl. Phys. **56**, 683 (1964).

[7] W. E. Lamb, Phys. Rev. **55**, 190 (1939).

[8] F. R. Metzger, Progr. Nucl. Phys. **7**, 53 (1959).

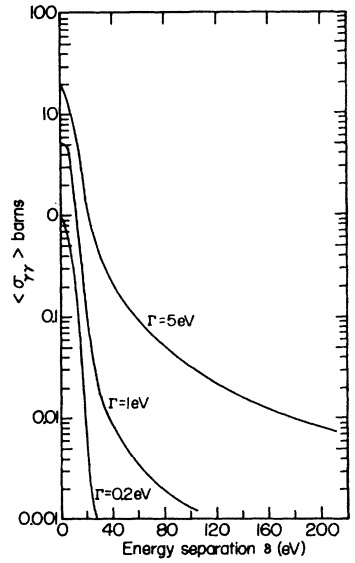

FIG. 4. Variation in effective cross section for resonant scattering $\langle\sigma_{\gamma\gamma}\rangle$ as a function of the energy separation δ. Nuclear levels are chosen having $g(\Gamma_0/\Gamma)^2$ equal to unity, and widths of 5, 1, and 0.2 eV.

ability that a gamma line falls within a distance δ of a given resonant level in the target nucleus is itself proportional to δ. The curves of Fig. 4 therefore describe the probability of observing a cross section greater than a certain value, in scattering of random-energy gamma lines from a given nuclear level. This probability is simply proportional to the abscissa δ, the proportionality factor depending on the density of gamma lines. It can be seen that the shapes of these probability distributions are not identical for different level widths. While they are very similar in the Doppler region, up to a few eV, at greater separations δ where the Breit-Wigner form predominates, the probability of smaller cross sections drops off far more rapidly for smaller values of Γ. In the example given, the level of width 5 eV has its cross section reduced by a factor of 1000 at a distance δ equal to 128 eV. The corresponding distance for the 0.2-eV level is 26 eV. It is clear that the detection of resonance scattering is greatly increased for broader nuclear levels, for not only is the actual cross section larger (important where an experimental cutoff exists) but also, owing to the increased sensitivity width, more gamma lines become available for resonance scattering.

For levels having similar nuclear properties, in a given nucleus, the experimental distribution in $\langle\sigma_{\gamma\gamma}\rangle$ could be expected to give information on the average levelwidth and possibly the statistical fluctuation in these levelwidths. No direct conclusions can be drawn however, for the combined distribution of effective cross sections for all the 45 measured resonances, since the resonances occur in different nuclei, for different sources, and in most cases the cross sections must be increased to take into account the isotopic abundance of the actual unknown isotope responsible for the resonance. As an illustration of a case where the latter uncertainty is reduced, Fig. 5 shows the combined distribution of effective cross sections for all the 11 resonances found in La and Pr, effectively mono-isotopic elements. The statistics are of course very poor, but the integral distribution seems to be in agreement with an exponential relationship. However even in this case the experimental distribution is a sum over a large number of distributions similar to those in Fig. 4, with differing nuclear parameters and Doppler widths, in addition to which there is the effect of the cutoff dictated by the experimental conditions. Because of the very poor statistics available per target nucleus in the present experiment, no direct conclusions can be drawn concerning the general level properties, except of course that the lower limit for the level widths can be calculated in each case assuming a separation $\delta=0$. If more sensitive experiments become possible, as discussed below, so that a large number of resonances can be observed for each target, valuable information could be found from the distribution in effective cross sections.

The above analysis has not taken into account the cutoff cross sections, denoted by σ_c, which depends upon the experimental conditions, particularly the intensity of the gamma line, the electronic cross section, and geometry of the scatterer. If the electronic total cross section is much greater than the nuclear effective cross section, σ_c is not dependent on the properties of the particular nuclear level involved. For the case where electronic absorption predominates, the effective cross section is determined experimentally using the follow-

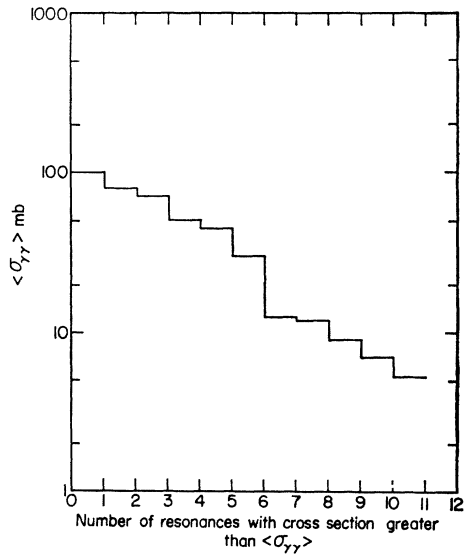

FIG. 5. Integral distribution of the effective cross sections for the 11 resonances in the mono-isotopic elements lanthanum and praseodymium.

ing Eq. (3),

$$\langle\sigma_{\gamma\gamma}\rangle=\frac{C_{sc}}{C_0}\frac{\eta_0}{\eta_{sc}}\frac{11.2}{\Delta\Omega}\left\{\frac{(1+\sqrt{2})\sigma_e}{1-\exp[-(1+\sqrt{2})\sigma_e N x_0]}\right\}, \quad (3)$$

where the parameters are as defined for Eq. (1). The expression in curly brackets is defined as the thickness parameter χ, and can be shown to vary slowly with energy over the range 5–9 MeV. χ is shown for each scatterer in Table II, for an energy of 7 MeV. The values of χ can be seen to be between 2 and 75 b, the majority being in the range 10–30 b; hence in order to examine average values of σ_c we have taken a typical value of 20 b for χ. More precise calculations for a particular scatterer must take into account the actual value of χ in each case. Substituting the experimental values for (η_0/η_{sc}) $11.2/\Omega$, averaged over the energy range, into Eq. (3) we find

$$\langle\sigma_{\gamma\gamma}\rangle=2460(C_{sc}/C_0)(\chi/20b). \quad (4)$$

The cutoff value σ_c is then found by substituting the value of C_0 for the particular gamma line, and the minimum detectable value of C_{sc} for that energy and the relevant background conditions. Both these quantities depend upon reactor power and the duration of the experiment. We have assumed a two-hour experiment at 2 MW, typical for the cross-section experiments carried out. The experimental values of C_0 for each individual gamma line were obtained by normalizing the integrated direct spectrum for each gamma source using the experimental detector response functions, and multiplying by the published tabulated line intensities.[5] These values of C_0 are shown in Fig. 6, where it can be seen that the intensities vary by over three orders of magnitude, with over 200 individual gamma lines contributing to the over-all line spectrum.

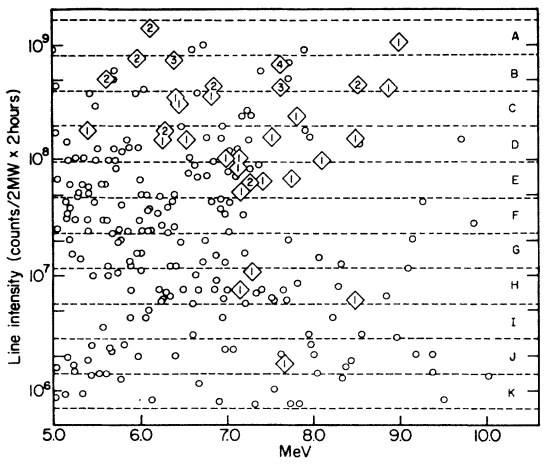

FIG. 6. Experimental intensity distribution of the capture gamma line sources as a function of energy. The various lines are divided into 11 intensity groups (A, B, $\cdots$, K), the mean intensity of adjacent groups differing by a factor of 2. ◇ denotes gamma lines giving resonance scattering, the figures denoting the number of resonances observed for that line.

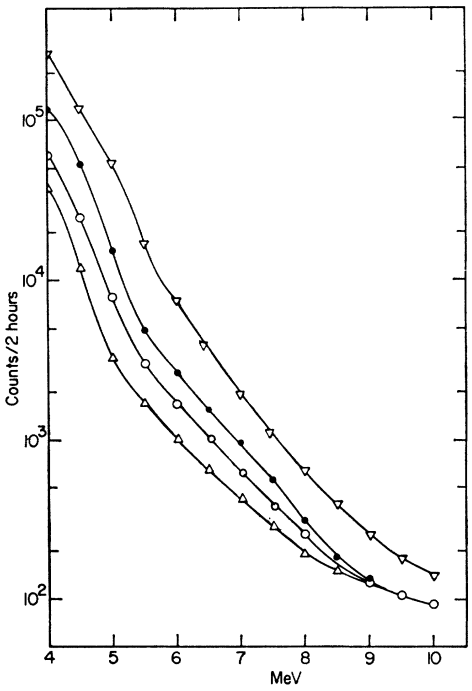

FIG. 7. Typical background curves for the four combinations of strong and moderate sources and low- and high-Z scatterers. ▽ Scatterer: Au; source: Cu: • Scatterer: P; source: Cu; ○ Scatterer: Bi; source: V; △ Scatterer: Mg; source V.

Undoubtedly many more lines of weaker intensity also exist, and the spectrum will require revision as more precise measurements and tabulations on capture gamma spectra are published. The spectrum in Fig. 6 has arbitrarily been divided into 11 different groups A, B, $\cdots$, K, according to intensity, the mean intensity of adjacent groups differing by a factor of 2. As the cross section is inversely proportional to C_0, the quantity σ_c is multiplied by a factor of 2 in going from one group to its neighbor in the direction of decreasing intensity.

The minimum detectable value C_{sc}(min) depends on the detector resolution and on nonresonant background intensity in the detector, itself a function of the particular combination of source and target. Typical background spectra are shown in Fig. 7, taking extreme conditions. The background depends strongly on the source intensity and target conditions, variations of up to a factor of 10 being found for the extreme conditions. Using the average values of the background, we have estimated C_{sc}(min) as a function of energy, and the results are shown in Fig. 8. As C_{sc}(min) varies approximately as the square root of the background intensity, the use of the average values at low energies introduces a possible error of a factor of 3 for the different source-target combinations used in the present experiment.

The calculated values of σ_c, based on the data of Figs. 6 and 8, are shown in Fig. 9 for three groups of

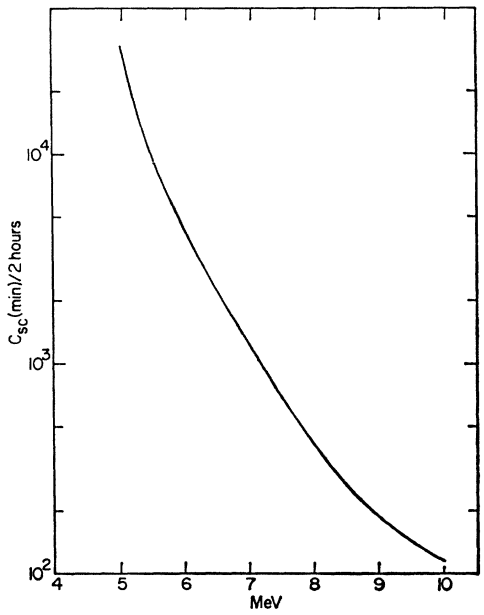

FIG. 8. Variation of C_{sc}(min), the minimum scattering intensity under the photopeak for detection of a resonance. Experimental conditions: 2 MW, 2 h counting time.

gamma rays. The values for any other gamma intensity group can be found by using the appropriate intensity. Comparing these values with the experimental cross sections summarized in Table III and Fig. 6, it can be seen that the great majority of resonances are due to gamma lines in groups A–E. Lines in groups with lower intensity than F could only detect

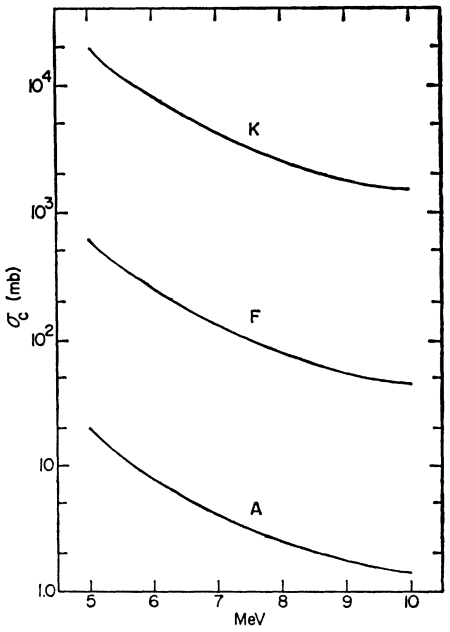

FIG. 9. Variation of the cutoff cross section σ_c as a function of energy, for three different gamma line intensities. The assignments A, F, and K are the same as in Fig. 6.

resonances having relatively large cross sections, which explains the small number of resonances observed in those groups.

It should be emphasized that because of the many approximations used, the above discussion on cutoff cross sections is only qualitative, but does give orders of magnitude of the sensitivity of the present experiment for the different source-target combinations. In addition these results can be used to predict the advantages expected from various modifications of the present experiment.

DISCUSSION

The pronounced resonance scattering found for elements in the region of closed shells has been discussed

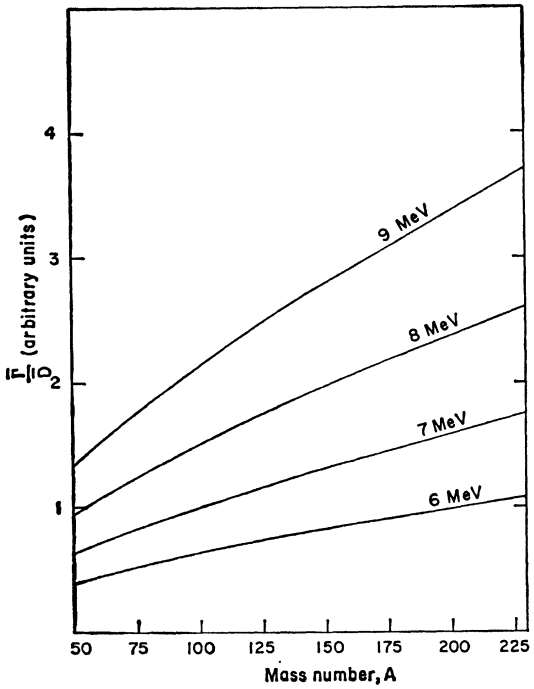

FIG. 10. Strength function according to Cameron as a function of the mass number A for different excitation energies E.

previously by Axel[9] and by the present authors.[2] Cameron[10] studied the behavior of the strength function $\bar{\Gamma}_0/\bar{D}$ as a function of energy and mass, and derived the following relationship:

$$\bar{\Gamma}_0/\bar{D}=CA^{2/3}E^3, \tag{5}$$

were $\bar{\Gamma}_0$ is the mean level width for decay to the ground state, $\bar{D}$ is the mean level separation and C is a constant. Using the above equation, the expected variation of $\bar{\Gamma}_0/\bar{D}$ is shown in Fig. 10 for different values of E and A.

[9] P. Axel, Phys. Letters 4, 320 (1963).
[10] G. W. Carmeron, Can. J. Phys. 35, 666 (1957).

The curves show a smooth variation with respect to A and no shell effects can be expected in the value of the strength function using Cameron's relation. However, it is known that heavy nuclei near or at closed shells have relatively larger level separations than nuclei far from closed shells, and hence, for a given strength function as given by the Cameron equation, they have larger values of the mean level width $\bar{\Gamma}_0$. Because of the experimental cutoff in the resonant scattering cross section the present experiment discriminates against low values of $\bar{\Gamma}_0$. More resonances would therefore be observed in the region of closed shells, where there are a few broad levels, than in nuclei between shells, having many narrow levels.

The low density of low-lying levels in the region of closed shells reduces the probability of a dipole transition to an excited state, thus giving a ground-state branching ratio ($\bar{\Gamma}_0/\Gamma$) close to unity for highly excited states below the neutron emission threshold. For nuclei far from closed shells this branching ratio is usually much less than unity, which greatly reduces the scattering cross section, and therefore the probability of observing resonant scattering from these nuclei.

Another effect favoring the observation of resonant scattering in nuclei with an even neutron number is the rapid drop in the branching ratio above the (γ,n) threshold. Since even-N nuclei have higher (γ,n) threshold energies than odd-N nuclei, they have an extended energy region for observation of resonance scattering. The rapid drop in the threshold energy for the heavy elements U and Th is in itself sufficient to explain the absence of observed resonance scattering above 5 MeV.

Using the above arguments, Axel predicted pronounced scattering for Pb, Hg, and Pt among the heavy element even-even nuclei, for Bi, Tl, Pr, La, and Y among the odd-Z even-N nuclei, and for Ba, Ce, Nd, Sr, Zr, Mo among the medium weight elements. These predictions are very well borne out by the experimental results presented here.

In favorable cases it has been possible to analyze individual resonances and to measure the level parameters Γ_0 and Γ. To do this a combination of several experimental techniques was used, including measurement of the effective cross section for resonance scattering and the changes due to temperature variation of the scattering target,[2] self-absorption technique,[2] and rapid rotation of the scattering target to give a Doppler energy shift to the gamma ray.[11] However, these methods are only applicable to resonances having a separation of less than 15–20 eV between the gamma line and the level energy, and because of the good statistics required, such measurements have only been carried out for the relatively few cases where a very large scattered intensity is available. Four cases have been reported in the literature[2,4,12,13] and the results do not permit any general conclusions to be drawn on the levelwidth distribution.

As discussed above, the observed distribution in effective cross sections does not permit any analysis of properties of the nuclear levels, because of the poor statistics available for any particular nucleus. However, the present experiment can be considerably improved in several ways. For example the gamma source can be strengthened by using a higher thermal neutron flux. An increase by a factor of 100 would in effect increase the efficiency of the experiment by a factor of 10, assuming that the background increases at the same rate. The use of such high-intensity sources would also permit the use of higher resolution Ge counters, this again reducing the cutoff cross section for determining resonance scattering. By introducing both of these improvements it is hoped to reduce the cutoff cross section by one or two orders of magnitude. The increase in the number of observed resonances then expected depends, of course, on the assumed level width distribution, and may be calculated from the derivation of the cutoff cross section given above, in conjunction with the Cameron relation. It is expected that for mono-isotopic targets in the closed-shell region these improvements will permit the identification of at least 100 levels per target in the energy region 5–9 MeV. It will then be possible to obtain valuable information on the level parameters of these nuclei, without the necessity of individual parameter analysis of each resonance.

The potentialities of the method described are clear, and it is hoped that resonant scattering using the random overlap between thermal neutron-capture gamma lines and highly excited nuclear levels can be developed as a powerful tool in nuclear spectroscopy.

[11] B. Arad, G. Ben-David, and Y. Schlesinger, Phys. Rev. **136**, B370 (1964).
[12] H. H. Fleischmann and F. W. Stanek, Z. Naturforsch. **18a** 555 (1963).
[13] H. H. Fleischmann and F. W. Stanek, Z. Physik **165**, 172 (1963).